

Evolutionary State-Space Model and Its Application to Time-Frequency Analysis of Local Field Potentials

Xu Gao^{*}, Babak Shahbaba^{*}, Norbert Fortin^{***}, and Hernando Ombao^{*,**}

^{*}Department of Statistics, University of California, Irvine, California, 92697

^{**}Department of Cognitive Sciences, University of California, Irvine, California, 92697

^{***}Center for the Neurobiology of Learning and Memory, Department of Neurobiology and Behavior, University of California Irvine, Irvine, California 92697

November 3, 2016

Abstract

We propose an evolutionary state space model (E-SSM) for analyzing high dimensional brain signals (in particular, local field potentials in rats) whose statistical properties evolve over the course of a non-spatial memory experiment. Under E-SSM, brain signals are modeled as mixtures of components with oscillatory activity at defined frequency bands. One unique feature of E-SSM is that the components are parametrized as second order autoregressive AR(2) processes. To account for the potential non-stationarity of these components (since the brain responses could vary throughout the entire experiment), the parameters are allowed to vary over epochs. In contrast to independent component analysis, the method for estimating the components in E-SSM accounts for the entire temporal correlation of the components. Moreover, compared to purely data-adaptive strategies, such as filtering, E-SSM easily accommodates non-stationarity through the component of AR parameters. To estimate the model parameters and conduct statistical inference, we use Kalman smoother, maximum likelihood and blocked resampling approaches. The E-SSM model is applied to a multi-epoch LFP signals from a rat in a non-spatial (olfactory) sequence memory task. Our method captures the evolution of the power for different components across phases

of the experiment. The E-SSM model also identifies clusters of electrodes that behave similarly with respect to the decomposition of different sources. These findings suggest that the activity of different electrodes changes over the course of the experiment. Treating these epoch recordings as realizations of an identical process could give rise to misleading results. The proposed model underscores the importance of capturing the evolution in brain responses during the course of an experiment.

Keywords: Auto-regressive model; brain signals; spectral analysis; state-space models; time-frequency analysis.

1 Introduction

1.1 Background

The goal of this paper is to develop a novel model for investigating how a brain process could evolve over the duration of a learning experiment. To infer brain neuronal activity, we shall use electrophysiological recordings such as local field potentials (LFPs) and electroencephalograms (EEGs) which indirectly measure electrical activity of neurons in animal brains. LFPs are electrical signals from a single or multiple electrodes that capture the integration of membrane currents in a local region of cortex (Mitzdorf et al., 1985).

In practice, LFPs are the observed spatio-temporal signals at different tetrodes. In our dataset, we have LFP recordings in a rat which are obtained from an implanted plate with 12 electrodes. LFPs can be characterized as mixtures of different underlying oscillatory processes and there have been a number of approaches used to estimate these latent independent sources (Whitmore and Lin, 2016; Einevoll et al., 2007). In a recent paper, Fiecas and Ombao (2016) study the dynamics of LFPs during the course of experiment via Cramér representations and hence does not investigate low dimensional representations which are indispensable to modeling these multi-electrode LFPs. Data-adaptive methods such as independent components analysis (ICA) and principal components analysis (PCA) provide estimates for the unobserved cortical sources. However, they do not provide rigorous modeling and inference for settings with multiple epochs, where the underlying sources have spectral structures that could change over the course of the experiment. In addition, these approaches may produce sources which are not easily interpretable, e.g., they may not represent sources with oscillations at precise frequency bands. Moreover, without any constraint on the structure of the sources, it is extremely difficult to pool information across the epochs in the experiment. To overcome these major limitations, we will develop the evolutionary state space model (E-SSM).

1.2 Preliminary analysis from an olfactory (non-spatial) sequence memory experiment

The proposed E-SSM was motivated by results from our preliminary analyses of LFPs in an olfactory (non-spatial) sequence memory experiment performed in a memory laboratory led by our co-author to study how neurons learn the sequential ordering of odors presented (see Allen et al. (2016)). As shown in Figure 1, rats were trained to identify a sequence of odors while electrophysiological signals were recorded. In Figure 2, LFPs signals from one electrode recorded from the first 15 epochs are plotted. We further study the behavior of these LFPs by examining their spectra. In Figure 3, we plot the boxplots of the log periodograms across all the epochs from one electrode. These reveal that LFPs contain power at distinct delta (0-4 Hertz), alpha (8-12 Hertz) and the high-beta low-gamma (30-35 Hertz) bands.

One key goal in this paper is to model how the LFPs signals evolve over the course of many epochs in the experiment as the rat learns the sequence of the odor presentation. As an exploratory step, we divided the session into early (Phase 1), middle (Phase 2) and late (Phase 3) phases. In each of these phases, we computed the average periodogram which is plotted on the left side of Figure 4. On the right side, we plot the relative periodogram (rescaling the periodogram so that the relative periodogram for each frequency sums to 1) and noted that the spectral power evolved during the course of experiment with the most dramatic changes happening on the last phase. During the early phase, power had a broad (rather than concentrated) spread across bands. However, at the late phase, power seems to have been more concentrated at the low beta and gamma bands. Our contribution here is the E-SSM model that explicitly captures this evolutionary behavior in high dimensional time series.

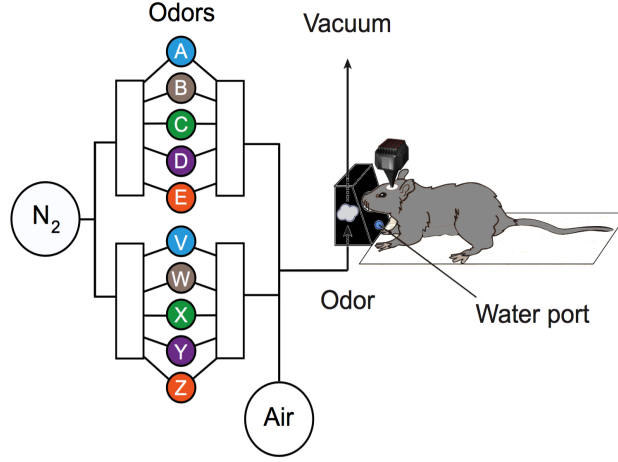


Figure 1: Apparatus and behavioral design for the olfaction (non-spatial) memory sequence experiment (Allen et al., 2016). Series of five odors were presented to rats from the same odor port. Each odor presentation was initiated by a nose poke. Rats were required to correctly identify whether the odor was presented in the correct or incorrect sequence position (by holding their nose in the port until the signal or withdrawing before the signal, respectively).

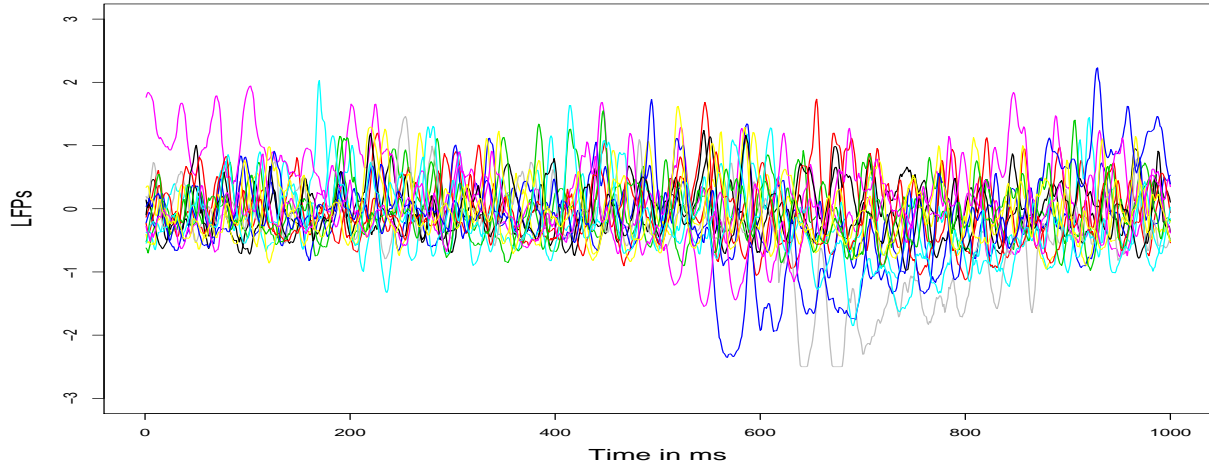


Figure 2: The overlaid time series LFPs plots of the first 15 epochs at electrode 7. The experiment and the data are reported in Allen et al. (2016).

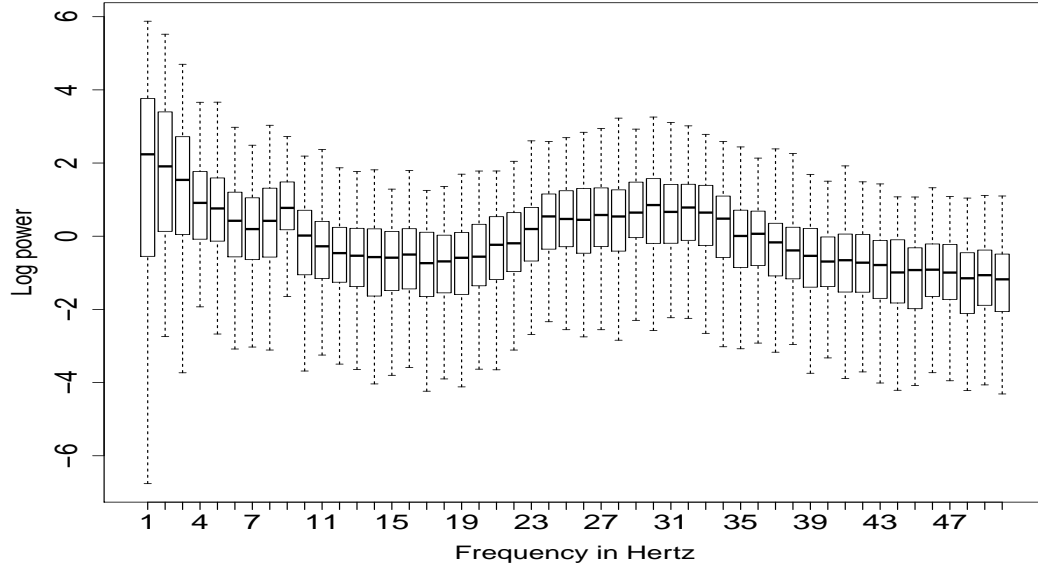


Figure 3: The log periodogram boxplots for each frequency obtained by all 247 epochs at electrode 7.

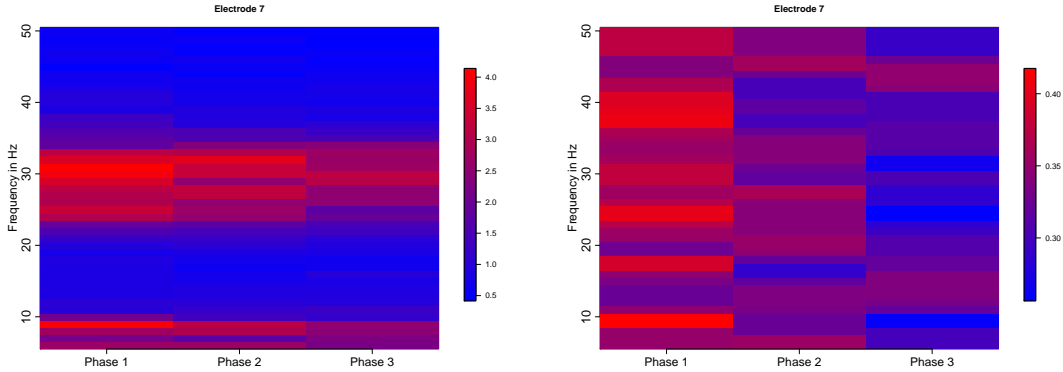


Figure 4: Left: The heatmap of the averaged periodogram among Phase 1 (epochs 1 - 80), Phase 2 (81 - 160) and Phase 3 (161 - 247) respectively at electrode 7. Right: The heatmap of the relative periodogram (summing up to 1 for each frequency). Spectral power (decomposition of waveform) evolved across phases of the experiment with the most dramatic effect captured by the last phase.

In summary, from the LFPs signals, we observe that there exists strong similarity of the LFP waveforms across many electrodes. Moreover, as shown in Figures 3 and 4, the

spectra of the LFPs appear to change across the epochs in the experiment. The proposed E-SSM model in fact explicitly takes into account both of these empirical observations about the LFP data. The E-SSM shares a similar form to the classical state-space model (as in (Shumway and Stoffer, 2013)) but differs in that the parameters are varying across epochs and the observational (or “mixing”) matrix is unknown and has to be estimated. Moreover, E-SSM captures the temporal correlation of each of the latent sources by characterizing these as second order autoregressive [AR(2)] processes. The reason for choosing AR(2) is clearly due to its ability to capture the precise oscillatory behavior of these sources. That is, by parameterizing these sources as AR(2), we can constrain the power of each source to these particular frequency bands: delta (0 - 4 Hertz), alpha (8 - 12 Hertz) and high-beta gamma (> 30 Hertz) bands. This is a clear advantage over the PCA and ICA methods since the sources produced by E-SSM are easily interpretable in terms of oscillatory properties.

1.3 Contributions

The main contributions of this paper are as follows: (1.) The proposed E-SSM model provides a rigorous framework in modeling the dynamics of brain activity and connectivity during the course of experiments. In particular, our model accounts for the temporal evolution/dependence of the spectrum power for particular frequency bands across the entire experiment. (2.) E-SSM accounts for the temporal structure among the latent sources. Specifically, the estimate of sources and hence of the auto spectrum in the current epoch takes into account the signals at neighboring epochs. (3.) E-SSM gives interpretable results by modeling particular predominant frequency bands that are associated with various brain functional states through these AR(2) processes. (4.) By applying the E-SSM model, one can easily conduct analysis on both of time and frequency domains and thus provide a complete characterization of the underlying brain process. (5.) Finally, the E-SSM model and the proposed estimation method, in general, are intuitive and easily implemented. They take advantage of existing theory and algorithm for state space model. However, the novelty of the proposed E-SSM is that it generalizes the state space framework to the multiple epochs

setting (borrowing information across epochs) and does not constrain the “mixing” matrix to be known.

1.4 Outline of the paper

The remainder of this paper is organized as follows. In Section 2, we develop a framework of the proposed method to model the variability across epochs while taking into account particular frequency bands. In Section 3, we propose a hybrid iterative method that comprises of Kalman filter and blocked resampling for estimating the “mixing” matrix and maximum likelihood (ML) for estimating the AR(2) parameters. In Section 4, we compare the existing methods (ICA and PCA) to the proposed E-SSM. In Section 5, we present some results to evaluate the performance on single-epoch and multiple-epoch scenarios. Results show the method is promising in reconstructing the latent source signals and their spectrum. In Section 6, we apply the proposed E-SSM to an LFPs dataset obtained from a nonspatial olfactory sequence memory study. Results demonstrate the evolution of the statistical property of the brain signals across the experiment - in particular on the varying spread or concentration of power. In addition, the analysis revealed a frequency-band specific clustering of the electrodes.

2 Evolutionary State Space Model (E-SSM)

As is discussed in Section 1, the proposed method is motivated by analyzing LFPs data obtained from a nonspatial sequence memory study. The objectives of the analysis are to model the latent structures in LFPs and to investigate how they evolve across epochs. In this section, we shall first describe the model for a single epoch and then develop this further to multiple epochs.

2.1 State Space Model for a single epoch

Denote $t = 1, \dots, T$ as the time points in a single-epoch experiment and $\mathbf{Y}_t = (Y_t(1), \dots, Y_t(p))'$, as the observed LFPs where p is the number of electrodes. For any fixed time point t , we assume that \mathbf{Y}_t is a *mixing* of latent independent source signals. Denote $\mathbf{S}_t = (S_t(1), \dots, S_t(q))'$ and q to be the number of spatial source signals, the model can be presented as $\mathbf{Y}_t = M\mathbf{S}_t + \boldsymbol{\epsilon}_t$, where M is the “mixing” matrix, $\boldsymbol{\epsilon}_t = (\epsilon_t(1), \dots, \epsilon_t(p))'$ are Gaussian noise that follows $N(\mathbf{0}, \tau^2 \mathbf{I}_p)$ and \mathbf{I}_p is an identity matrix of dimension p . Each of the independent latent signals $S_t(l), l = 1, \dots, q$ models the source that represents oscillatory activity at the common frequency bands (delta, alpha and gamma).

On modeling the source signals \mathbf{S}_t

One unique parameterization in this model is to constrain the sources to have an AR(2) structure so that they represent the delta, theta, alpha and gamma oscillations. We will start with stating some basic concepts in time series.

Definition 1. The autocovariance function $\gamma(h)$ of a weakly stationary time series x_t with $\mathbb{E}(x_t) = 0$ is defined as $\gamma(h) = \text{Cov}(x_{t+h}, x_t)$, for any time t and lag h .

Definition 2. A zero mean stationary time series x_t follows an autoregressive model of order p , denoted $AR(p)$, if it is of the form $x_t = \phi_1 x_{t-1} + \phi_2 x_{t-2} + \dots + \phi_p x_{t-p} + w_t$, where ϕ_1, \dots, ϕ_p are parameters, w_t is a Gaussian white noise series with mean zero and variance σ_w^2 .

Definition 3. The autoregressive operator (autoregressive polynomial) is defined to be

$$\phi(B) = 1 - \phi_1 B - \phi_2 B^2 - \dots - \phi_p B^p, \quad (1)$$

where B is a backshift operator defined by $B^\ell x_t = x_{t-\ell}$.

On the frequency domain, we define the spectral density as follows

Definition 4. Let $f(\omega)$ be the spectrum of a stationary process with corresponding autocovariance function, $\gamma(h)$, which is absolutely summable. Then $\gamma(h)$ and $f(\omega)$ are defined as follows: $\gamma(h) = \int_{-1/2}^{1/2} e^{2\pi i \omega h} f(\omega) d\omega$, $h = 0, \pm 1, \dots$ and $f(\omega) = \sum_{h=-\infty}^{\infty} \gamma(h) e^{-2\pi i \omega h}$, $-\frac{1}{2} \leq \omega \leq \frac{1}{2}$.

As a special example, the spectrum of an $AR(2)$ process is $f(\omega) = \frac{\sigma_w^2}{|1 - \phi_1 \exp(-2\pi i \omega) - \phi_2 \exp(-4\pi i \omega)|^2}$. To illustrate this idea, Figure 5 shows the spectrum of $AR(2)$ process with $\phi_1 = 1.976$, $\phi_2 = -0.980$, $\sigma_w = 0.1$. It can be seen that there is a peak at a band around frequency $\omega = 10$ Hertz. So, we can conclude that the frequency $\omega = 10$ Hertz dominates the process and thus produces the most power. This property of $AR(2)$ time series models makes it potentially useful for characterizing brain signals (such as LFPs) with oscillatory behavior.

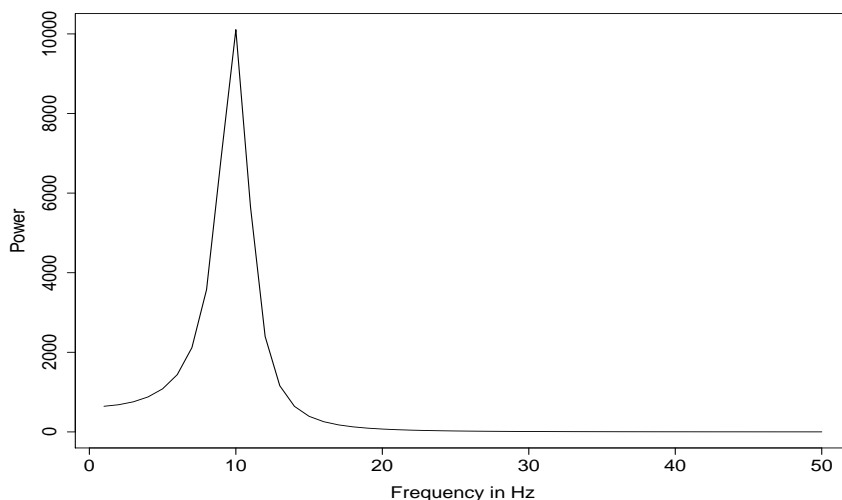


Figure 5: The theoretical spectra of an $AR(2)$ process with power concentrated at the alpha band: $\phi_1 = 1.976$, $\phi_2 = -0.980$, $\sigma_w = 0.1$ (alpha frequency band).

We now explain the connection between the $AR(2)$ coefficients and the spectrum (i.e., the location and spread of the peak). First, the process is causal when the roots of the polynomial in Equation (1) have magnitudes greater than 1. Furthermore, under causality, Jiru (2008) and Shumway and Stoffer (2013) demonstrate that when the roots of the polynomial in Equation (1) are complex-valued with magnitude greater than 1, then the spectrum attains

a peak that is located at the phase of the roots. Moreover, when the magnitude of the roots become larger than 1, the peak becomes less concentrated around the phase. Motivated by this result, we will fix the phase (or argument) of each of the $AR(2)$ polynomial roots to model each of the particular bands. To model the evolution across epochs, we allow the module of the $AR(2)$ polynomial roots changes among epochs. As a result, after we fix the arguments of the roots for each of the latent independent source signals, the $AR(2)$ process is uniquely determined by the modulus and the variance. In practice, the value of modulus controls the spread of the spectrum curves. For an $AR(2)$ process $x_t = \phi_1 x_{t-1} + \phi_2 x_{t-2} + w_t$, the modulus ρ and phase ψ of the roots of the polynomial have the relationship that $\phi_1 = 2\rho^{-1}\cos(\psi)$, $\phi_2 = -\rho^{-2}$.

Following the previous discussion, the latent independent spatial source signals are modeled as multivariate autoregressive processes of order 2, $\mathbf{S}_t = \Phi_1 \mathbf{S}_{t-1} + \Phi_2 \mathbf{S}_{t-2} + \boldsymbol{\eta}_t$, where $\Phi_1 = \text{diag}(\phi_{11}, \dots, \phi_{q1})$, $\Phi_2 = \text{diag}(\phi_{12}, \dots, \phi_{q2}) \in \mathbb{R}^{q \times q}$ are diagonal matrices and noise is independent Gaussian to guarantee the independence of the sources, $\boldsymbol{\eta}_t = (\eta_1(t), \dots, \eta_q(t))'$ are Gaussian noise that follows $N(\mathbf{0}, \sigma^2 \mathbf{I}_q)$ and \mathbf{I}_q is an identification matrix of dimension q .

Finally, the model can be generalized as state-space model as

$$\begin{aligned} \mathbf{Y}_t &= \widetilde{\mathbf{M}} \mathbf{X}_t + \boldsymbol{\epsilon}_t, \\ \mathbf{X}_t &= \widetilde{\Phi} \mathbf{X}_{t-1} + \widetilde{\boldsymbol{\eta}}_t, \end{aligned} \tag{2}$$

where $\mathbf{X}_t = (\mathbf{S}'_t, \mathbf{S}'_{t-1})'$, $\widetilde{\mathbf{M}} = (M, \mathbf{0}) \in \mathbb{R}^{p \times 2q}$, $\widetilde{\Phi} = \begin{bmatrix} \Phi_1 & \Phi_2 \\ \mathbf{I}_q & \mathbf{0} \end{bmatrix}$, and $\widetilde{\boldsymbol{\eta}}_t = (\boldsymbol{\eta}'_t, \mathbf{0})'$. Note that model in Equation (2) is not a regular state-space model since the “mixing” matrix $\widetilde{\mathbf{M}}$ is fixed but unknown. Moreover, following the aforementioned discussion, the coefficients of the autoregressive processes are determined by the modulus $\boldsymbol{\rho} = (\rho_1, \dots, \rho_q)$ and arguments $\boldsymbol{\psi} = (\psi_1, \dots, \psi_q)$ of the autoregressive polynomial roots. Since we are interested in particular frequency bands, we fix the argument $\boldsymbol{\psi}$ and the state equation in (2) is parameterized by $\boldsymbol{\rho}$ and σ^2 .

2.2 Evolutionary State Space Model for multiple epochs

In this section, we will generalize the proposed method in Section 2.1 to multiple epochs. We assume that across epochs, the mixing matrix M is fixed and the latent independent autoregressive processes evolve through the modulus ρ . This assumption is based on the cortical structure remains unchanged across epochs for each individual. We denote $r = 1, \dots, R$ as the epochs of conducting an experiment, then the model is expressed by

$$\begin{aligned}\mathbf{Y}_t^{(r)} &= \widetilde{M} \mathbf{X}_t^{(r)} + \boldsymbol{\epsilon}_t^{(r)}, \\ \mathbf{X}_t^{(r)} &= \widetilde{\Phi}^{(r)} \mathbf{X}_{t-1}^{(r)} + \widetilde{\boldsymbol{\eta}}_t^{(r)},\end{aligned}\tag{3}$$

where the definition of $\mathbf{Y}_t^{(r)}, \widetilde{M}, \mathbf{X}_t^{(r)}, \widetilde{\Phi}^{(r)}, \boldsymbol{\epsilon}_t^{(r)}, \widetilde{\boldsymbol{\eta}}_t^{(r)}$ are similar as in Equation (2) except that the superscript r accounts for epochs.

Remark 1. In this model, we assume that the autoregressive structure evolves across epochs. This assumption is inspired by the preliminary analysis in Section 1 showing that the power spectrum evolves during the course of the experiment. Accordingly, the evolutionary spectrum of each latent source will be easily captured throughout the model fitting. In particular, the theoretical evolutionary spectrum will be denoted as $f^{(r)}(\omega) = \frac{\sigma_w^{2(r)}}{|1 - \phi_1^{(r)} \exp(-2\pi i \omega) - \phi_2^{(r)} \exp(-4\pi i \omega)|^2}$.

Remark 2. Moreover, the “mixing” matrix is invariant to epochs. This is due to the fact that the network structure of subjects is not changing across phases of experiments.

Remark 3. Finally, note that $\widetilde{\Phi}^{(r)}$, which are uniquely determined by the evolving modulus and unchanged arguments of the autoregressive polynomial roots, evolves as r changes.

Remark 4. On identifiability issues. There has been numerous discussions on the identifiability issues of state-space models, e.g. model (2). Hamilton (1994) pointed out that “in the absence of restrictions on $\widetilde{M}, \widetilde{\Phi}, \sigma, \tau$, the parameters of the state-space representation are unidentified - more than one set of values for the parameters can give rise to the identical value of the likelihood function, and the data give us no guide for choosing among these”. Indeed, for a general state-space model, the representation can also be obtained by multiplying each of the equation by a orthogonal matrix. Arun and Kung (1990) stated this

issue and provided restriction to avoid this issue. Zhang and Hyvärinen (2011) proposed a non-Gaussian constraint to maintain the model identifiable. In this study, we address this problem by assuming that each component of the latent independent source signals $\mathbf{S}(t)$ have unit variance and the entries of $\widetilde{\mathbf{M}}$ is positive.

3 Estimation Method for E-SSM

In this section, we will provide algorithms/strategies for estimating parameters in the models proposed in Section 2.

Estimating E-SSM for a single epoch

To make inference of the proposed model (2), we propose an iterative algorithm that comprises of Kalman filter and least square estimates. We start with initial values $\widetilde{\mathbf{M}} = \widetilde{\mathbf{M}}_0$, \mathbf{X}_0^0 and P_0^0 . The whole procedure takes iterations between Algorithms 1 and 2 (shown below) until convergence.

Algorithm 1 Kalman Filter and Maximum Likelihood

```

1: procedure GIVEN  $\widetilde{\mathbf{M}}, \mathbf{X}_0^0, P_0^0$ , ESTIMATE  $\boldsymbol{\rho}, \sigma^2, \tau^2$  BY KALMAN FILTER AND MAXIMUM LIKELIHOOD OF INNOVATIONS  $\boldsymbol{\epsilon}_t$ 
2:   A.1 Kalman filter and Kalman gain step
3:    $\Phi_1 \leftarrow \text{diag}(2\rho_1^{-1}\cos(\psi_1), \dots, 2\rho_q^{-1}\cos(\psi_q))$ 
4:    $\Phi_2 \leftarrow \text{diag}(-\rho_1^{-2}, \dots, -\rho_q^{-2})$ 
5:    $\widetilde{\Phi} \leftarrow \begin{bmatrix} \Phi_1 & \Phi_2 \\ \mathbf{I}_q & \mathbf{0} \end{bmatrix}$ 
6:   for  $t = 0, \dots, T$  do
7:      $\mathbf{X}_t^{t-1} \leftarrow \widetilde{\Phi} \mathbf{X}_{t-1}^{t-1}$ 
8:      $P_t^{t-1} \leftarrow \widetilde{\Phi} P_{t-1}^{t-1} \widetilde{\Phi}' + \sigma^2 \begin{bmatrix} \mathbf{I}_q & \mathbf{0} \\ \mathbf{0} & \mathbf{0} \end{bmatrix}$ 
9:      $K_t \leftarrow P_t^{t-1} \widetilde{\mathbf{M}}' [\widetilde{\mathbf{M}} P_t^{t-1} \widetilde{\mathbf{M}}' + \tau^2 \mathbf{I}_p]^{-1}$  ▷ The Kalman gain
10:     $\mathbf{X}_t^t \leftarrow \mathbf{X}_t^{t-1} + K_t (\mathbf{Y}_t - \widetilde{\mathbf{M}} \mathbf{X}_t^{t-1})$ 
11:     $P_t^t \leftarrow (\mathbf{I}_{2q} - K_t \widetilde{\mathbf{M}}) P_t^{t-1}$ 
12:   A.2 Maximum likelihood estimation
13:   for  $t = 0, \dots, T$  do
14:      $\boldsymbol{\epsilon}_t \leftarrow \mathbf{Y}_t - \widetilde{\mathbf{M}} \mathbf{X}_t^{t-1}$ 
15:      $\Sigma_t \leftarrow \widetilde{\mathbf{M}} P_t^{t-1} \widetilde{\mathbf{M}}' + \tau^2 \mathbf{I}_p$ 
16:      $l_Y(\boldsymbol{\rho}, \sigma^2, \tau^2) \leftarrow \frac{1}{2} \sum_{t=1}^T \log |\Sigma_t| + \frac{1}{2} \sum_{t=1}^T \boldsymbol{\epsilon}_t' \Sigma_t^{-1} \boldsymbol{\epsilon}_t$  ▷ The negative loglikelihood
17:      $(\hat{\boldsymbol{\rho}}, \hat{\sigma}^2, \hat{\tau}^2) \leftarrow \underset{(\boldsymbol{\rho}, \sigma^2, \tau^2)}{\text{argmin}} l_Y(\boldsymbol{\rho}, \sigma^2, \tau^2)$  ▷ Maximizing the likelihood of innovations
   return  $\hat{\boldsymbol{\rho}}, \hat{\sigma}^2, \hat{\tau}^2$ 

```

Remark 5. In this study, since we are interested in the power of particular frequency bands, we will introduce box constraints to the modulus ρ_1, \dots, ρ_q to control the spread of the

spectra curves. Hence in A.2 of Algorithm 1, we implement an optimization method with box constraints on modulus ρ_1, \dots, ρ_q and no constraints on σ^2, τ^2 .

Algorithm 2 Kalman Filter and Least Squares Estimation

```

1: procedure GIVEN THE CURRENT ESTIMATES OF  $\rho, \sigma^2, \tau^2$ , WE CAN OBTAIN THE ESTIMATES OF  $\widetilde{M}$  BY KALMAN FILTER AND
   LEAST SQUARES ESTIMATION.
2:   B.1 Kalman filter and Kalman gain step
3:    $\Phi_1 \leftarrow \text{diag}(2\rho_1^{-1}\cos(\psi_1), \dots, 2\rho_q^{-1}\cos(\psi_q))$ 
4:    $\Phi_2 \leftarrow \text{diag}(-\rho_1^{-2}, \dots, -\rho_q^{-2})$ 
5:    $\widetilde{\Phi} \leftarrow \begin{bmatrix} \Phi_1 & \Phi_2 \\ \mathbf{I}_q & \mathbf{0} \end{bmatrix}$ 
6:   for  $t = 0, \dots, T$  do
7:      $\mathbf{X}_t^{t-1} \leftarrow \widetilde{\Phi} \mathbf{X}_{t-1}^{t-1}$ 
8:      $P_t^{t-1} \leftarrow \widetilde{\Phi} P_{t-1}^{t-1} \widetilde{\Phi}' + \sigma^2 \begin{bmatrix} \mathbf{I}_q & \mathbf{0} \\ \mathbf{0} & \mathbf{0} \end{bmatrix}$ 
9:      $K_t \leftarrow P_t^{t-1} \widetilde{M}' [\widetilde{M} P_t^{t-1} \widetilde{M}' + \tau^2 \mathbf{I}_p]^{-1}$  ▷ The Kalman gain
10:     $\mathbf{X}_t^t \leftarrow \mathbf{X}_t^{t-1} + K_t (\mathbf{Y}_t - \widetilde{M} \mathbf{X}_t^{t-1})$ 
11:     $\mathbf{X}_t^t \leftarrow \mathbf{X}_t^t / \text{sd}(\mathbf{X}_t^t)$  ▷  $\text{sd}(\mathbf{X}_t^t)$  denotes the standard deviation of  $\mathbf{X}_t^t$ 
12:    //Remark: We scale  $\mathbf{X}_t^t$  to unit variance for identifiability issues discussed before.
13:     $P_t^t \leftarrow (\mathbf{I}_{2q} - K_t \widetilde{M}) P_t^{t-1}$ 
14:   B.2 Least square estimation from Equation (2)
15:    $\mathbf{Y} \leftarrow (\mathbf{Y}_1, \dots, \mathbf{Y}_T)$  ▷  $\mathbf{Y} \in \mathbb{R}^{p \times T}$ 
16:    $\mathbf{X} \leftarrow (\mathbf{X}_1^1, \dots, \mathbf{X}_T^T)$  ▷  $\mathbf{X} \in \mathbb{R}^{q \times T}$ 
17:   for  $w = 1, \dots, p$  do
18:      $\widetilde{M}_w \leftarrow (\mathbf{X} * \mathbf{X}')^{-1} * \mathbf{X} * \mathbf{Y}'_{(w)}$  ▷  $\mathbf{Y}_{(w)}$  denotes the  $w$ th row of  $\mathbf{Y}$ 
19:    $\widetilde{M} \leftarrow (\widetilde{M}_1, \dots, \widetilde{M}_w)'$ 
   return  $\widetilde{M}$ 

```

Estimating E-SSM for multiple epochs

We propose a blocked resampling based approach to conduct inference on model (3). Here is the key idea: we obtain blocks of epochs; for each block we estimate the mixing matrix and the epoch-specific AR(2) parameters. These blocks retain the temporal sequence of the epochs and the final estimate at a previous epoch serves as the initial estimate of mixing matrix at the current epoch. The final estimates of the mixing matrix obtained from each block are averaged to produce the estimate for the common mixing matrix. As the next step, given the estimate of mixing matrix, we follow Algorithm 1 to obtain estimates of the epoch-specific AR(2) parameters. The iterative approach is summarized below.

II.A. We fix the length of the blocked resampling sampler as l . We draw the starting epoch index s from the set $\{1, 2, \dots, R - l + 1\}$. Then at current iteration, the blocked resampling sampler is $(\{\mathbf{Y}_t^{(s)}\}_{t=1}^T, \dots, \{\mathbf{Y}_t^{(s+l-1)}\}_{t=1}^T)$

A.1. Starting with epoch s , we implement the approach for single epoch in Section 2.1 on $\{\mathbf{Y}_t^{(s)}\}_{t=1}^T$ to obtain estimates $\widetilde{M}^{(s)}$.

A.2. Starting with epoch $s + 1$ and the initial value $\widetilde{M}^{(s)}$, we repeat A.1 to obtain estimates $\widetilde{M}^{(s+1)}$.

A.3. We repeat A.2 until the last epoch $s + l - 1$. We denote the final estimates $\widetilde{M}^{(s+l-1)}$ as the ultimate estimates of resampling sampler $(\{\mathbf{Y}_t^{(s)}\}_{t=1}^T, \dots, \{\mathbf{Y}_t^{(s+l-1)}\}_{t=1}^T)$. The pipeline of the procedure is summarized below.

$$\begin{bmatrix} \mathbf{Y}_1^{(s)} \\ \mathbf{Y}_2^{(s)} \\ \dots \\ \mathbf{Y}_T^{(s)} \end{bmatrix} \rightarrow \widetilde{M}^{(s)} \rightarrow \begin{bmatrix} \mathbf{Y}_1^{(s+1)} \\ \mathbf{Y}_2^{(s+1)} \\ \dots \\ \mathbf{Y}_T^{(s+1)} \end{bmatrix} \rightarrow \widetilde{M}^{(s+1)} \dots \rightarrow \begin{bmatrix} \mathbf{Y}_1^{(s+l-1)} \\ \mathbf{Y}_2^{(s+l-1)} \\ \dots \\ \mathbf{Y}_T^{(s+l-1)} \end{bmatrix} \rightarrow \widetilde{M}^{(s+l-1)}$$

II.B. Repeat II.A until a sufficient number of resampling estimates is obtained. Compute the average of those estimates, defined by \widetilde{M}_g , as the global estimate of \widetilde{M} .

II.C. Plug the global estimate \widetilde{M}_g into every single epoch. Following Algorithm 1 for single epoch discussed in Section 2.1, obtain the estimates of $\boldsymbol{\rho}^{(r)}, \sigma^{2(r)}, \tau^{2(r)}, r = 1, \dots, R$.

The over-all work flow is given in Figure 6. Note that since the “mixing” matrix \widetilde{M} are the same across epochs, we use the blocked resampling strategy to get the global estimates sequentially. Given that estimate, we proceed to make inference on every single epoch.

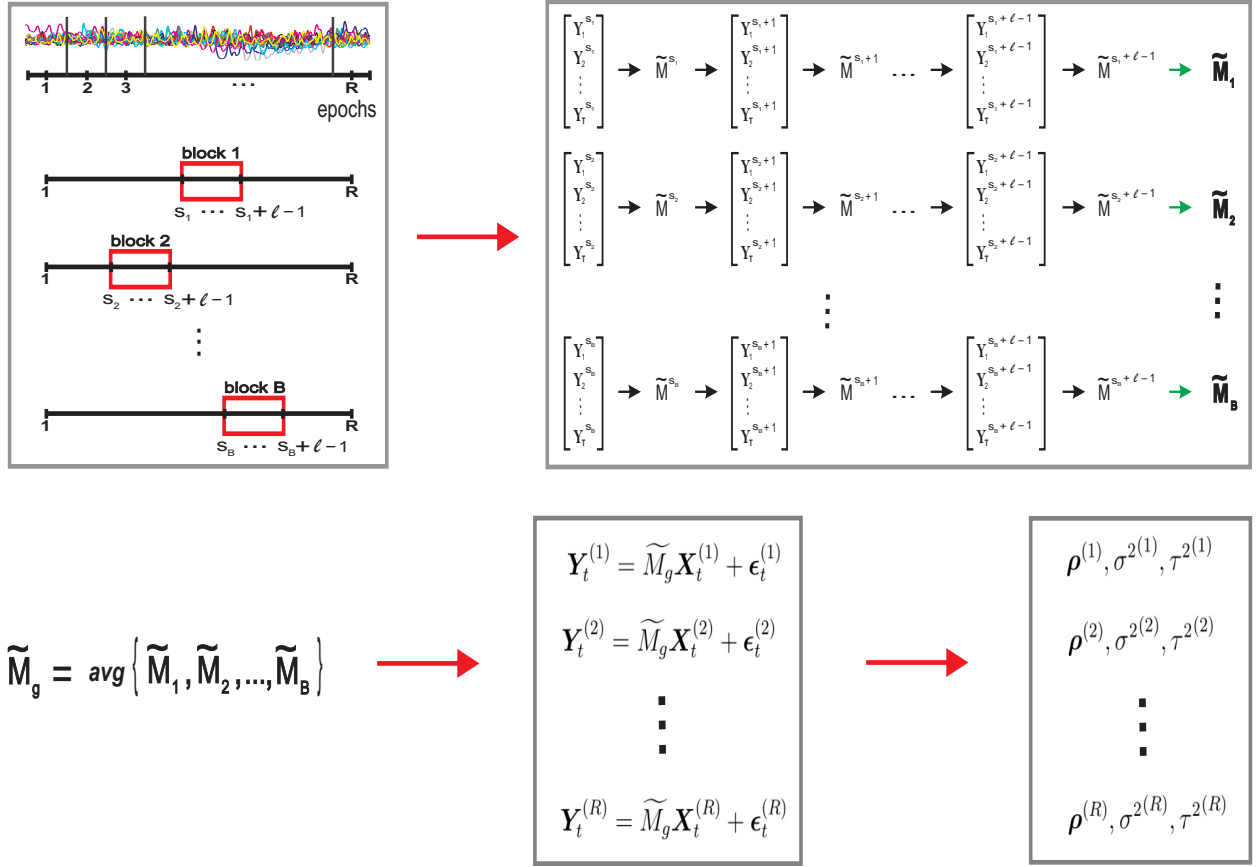


Figure 6: Schematic illustration of the estimation methods that summarize II.A, II.B and II.C in Section 2.2.

Remark 6. The blocked resampling method is utilized to estimate model (3) for the following reasons: (1.) Within each block, we utilize all the information sequentially to learn the same “mixing” matrix and break up the over-all computational burden. (2.) The optimization procedure may rely on initial values due to the complex structure of the model. However, using the blocked resampling method will avoid the sensitivity to starting values. (3.) We will obtain a distribution of the estimates of “mixing” matrix, which provides more flexibility for inference and an approach to test the stability of the proposed algorithm.

4 A Comparison to Existing Methods

Independent component analysis (ICA) is a general framework that has been widely used in modeling spatio-temporal data. It is a dimensionality reduction approach that assumes the signals are non-Gaussian and maximally statistically independent (Calhoun et al., 2009). Unlike principal component analysis (PCA) that assumes the sources are uncorrelated, ICA ensures the independence structure that allows for estimates of high-order statistics. The objective of ICA, in general, is to “recover” those independent non Gaussian latent structures. Bell and Sejnowski (1995) and Hyvärinen et al. (2004) proposed various algorithms to achieve that goal. ICA has been widely used in single/between-subject electrophysiological exploratory analysis. Makarova et al. (2011) proposed an ICA method to segregate pathways with partially overlapped synaptic territories from hippocampal LFPs. To investigate the variability across different subjects or subgroups, Guo (2011) proposed a general group probabilistic ICA (pICA) framework accommodating cross-subject structure in multisubject spatial-temporal brain signals. Maximum likelihood, exact EM and variational approximation EM algorithms were developed to estimate the parameters in the model.

The limitations of the existing (group) ICA methods for analyzing electrophysiological signals are the following. First, they do not have a mechanism for capturing how the parameters (and spectral properties) of the latent source signals may evolve across epochs over the entire experiment. Most of the existing methods are based on concatenating the signals from different epochs and estimating the parameters of the model as though these signals were realizations of the same underlying process. However, since the “reconstructed” latent sources vary across epochs, there is no rigorous framework for modeling how these parameters could change across epochs. As demonstrated in our exploratory analysis, Figure 3 and 4 show that the power of LFP signals changes quite drastically from the middle phase to the late phase of the experiment. Simply lumping together signals that are generated from different underlying source processes could yield misleading results. Second, the existing methods do not take into account the temporal structure of the latent sources. In fact, these sources are estimated for each time point independently of the other time points. Third,

given that spectral analysis of electrophysiological signals yield interpretable results, it is interesting that the current ICA methods for source modeling do not rigorously take this into account. In fact, brain researchers have observed association between power at different frequency bands and brain functional states (Michel et al., 1992). Thus, it is necessary to develop a framework that accounts for the evolution of the power at these frequency bands over many epochs. Lastly, there are limitations in the connection between time and frequency domain analysis. Methods from time and frequency domain are developed almost exclusively from each other which is counter-intuitive since these two approaches ought to be used concurrently in order to give a complete characterization of brain processes.

The proposed E-SSM was inspired by ICA and classical state-space model. Specific refinements and extensions were needed for the E-SSM in order to address to overcome the limitations of the current approaches and provide a framework that capture the dynamics on time and frequency domains.

5 Simulation Studies

5.1 Results on single epoch analysis

In this section, we will evaluate the proposed E-SSM on single epoch data. For the latent independent source signals, we assume that there are three $AR(2)$ stationary processes. Each of them corresponds to delta (δ : 0 - 4 Hertz), alpha (α : 8 - 12 Hertz), beta (β : 12 - 18 Hertz) frequency bands respectively. We randomly generate a positive “mixing” matrix M and fix the number of electrodes of the observational brain signals to be 20. In summary, following the notation in Section 2.1, we have: $p = 20, T = 1000, q = 3, \tau^2 = 1, \sigma^2 = .1, (\rho_1, \psi_1) = (1.0012, 2), (\rho_2, \psi_2) = (1.0012, 8), (\rho_3, \psi_3) = (1.0012, 15)$.

We implemented the proposed method in Section 2.1 and evaluated its performance. Figure 7 shows the periodograms of the true and reconstructed signals. As we can see, the estimated source signals share exactly the same shape as the true signals.

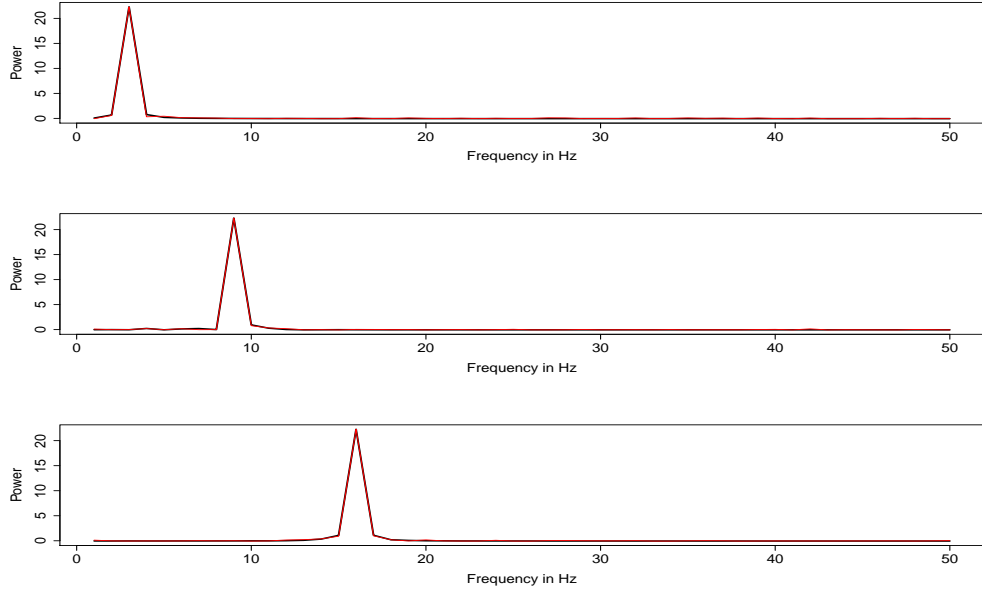


Figure 7: The periodograms of the true (black) and estimated (red) latent processes.

5.2 Results on multiple epoch analysis

In this section, we will evaluate the performance of the proposed method in Section 2.2. We choose 20 electrodes and 3 latent independent $AR(2)$ processes. To model the evolution across epochs, we allow the modulus $(\rho_1^{(r)}, \rho_2^{(r)}, \rho_3^{(r)})$ increase from $(1.001, 1.001, 1.001)$ with increment 0.00005 as the epoch r propagates. All the remaining parameters are the same as in Section 5.1. To visualize the signals, Figure 8 shows the heatmap of periodogram from electrode 1 as epochs evolve.

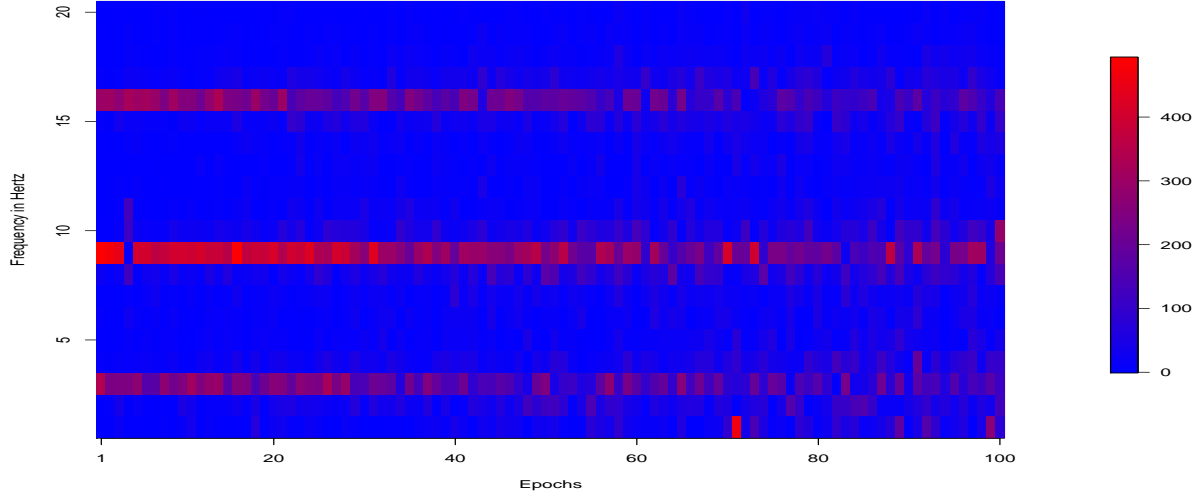


Figure 8: The periodogram of generated signals from electrode 1 computed over all 100 epochs. From the heat map, we are observing the powers are evolving across epochs. At early stage, three dominating frequency bands can be identified clearly. As epoch evolves, such pattern is getting less clear.

After we implement the method in this scenario, we find results similar to Section 5.1. Figure 9 shows the periodograms of the true and estimated signals from the three underlying $AR(2)$ processes. For the delta, alpha, and beta bands, we can see the peaks at the corresponding dominating frequency from the true and estimated signals. As the epochs evolve, we could observe that both of the true and estimated periodograms spread out around the dominating frequency. Our results show that the pattern of the periodograms from the reconstructed $AR(2)$ process is consistent with that of the true $AR(2)$ process.

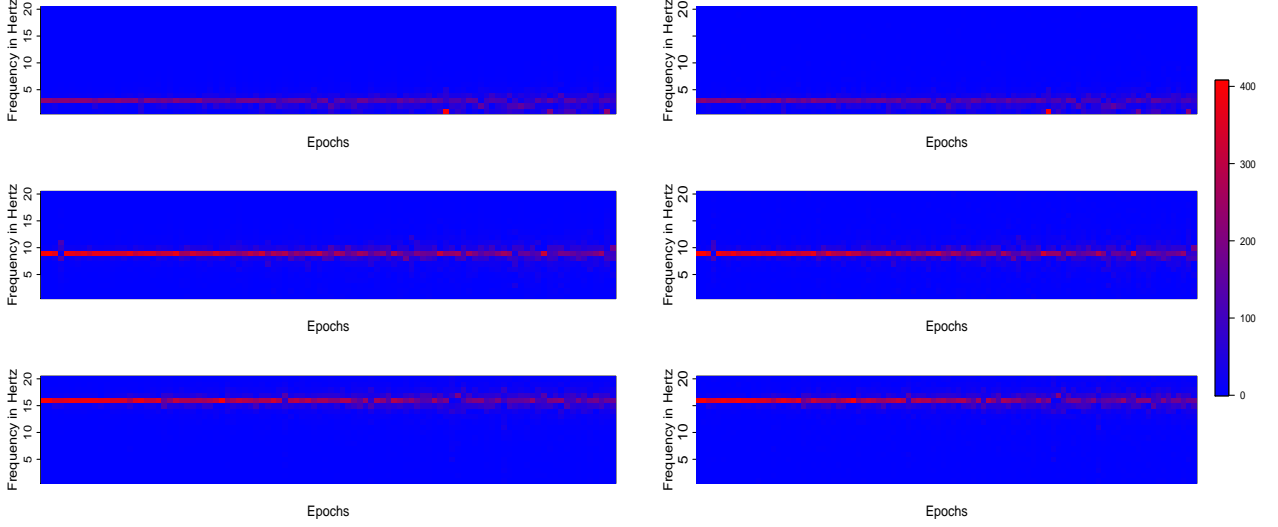


Figure 9: The periodograms of the true (left) and estimated (right) latent $AR(2)$ processes corresponding to delta (top), alpha (middle) and beta (bottom) frequency band.

5.3 Results from settings derived from the data

In this simulation study, we used the estimates of modulus, “mixing” matrix and variance parameters from the LFP data in the olfaction (nonspatial) sequence memory study to simulate the data. In particular, we used the estimates $(\hat{\rho}_1^{(r)}, \hat{\rho}_2^{(r)}, \hat{\rho}_3^{(r)}, \hat{\sigma}^{2(r)}, \hat{\tau}^{2(r)})$ and the estimate of “mixing” matrix \widetilde{M} to generate signals across 12 electrodes among 247 epochs. To test the performance of E-SSM, we also applied the classical state space model (SSM) estimation methods as a benchmark in comparison with E-SSM. Specifically, we worked on the state space model for each single epoch and take average to obtain parameters estimates, $(\hat{\rho}_1^{(r)}, \hat{\rho}_2^{(r)}, \hat{\rho}_3^{(r)}, \hat{\sigma}^{2(r)}, \hat{\tau}^{2(r)})$ as well as the estimate of the “mixing” matrix, \widetilde{M} . Note that this is the approach that most of the existing methods will follow when analyzing signals with multiple epochs.

We compare mean of sum of square errors of the parameters obtained from E-SSM and the benchmark. From Table 1, it is clear that E-SSM successfully captures the evolution of parameters compared to classical state space models. Among all the frequency bands,

the benefits are dramatic. These results highlight the advantages of using E-SSM when signals are comprised of multiple epochs. Meanwhile, it also indicates the potential loss of information if we naively average over all the epochs when conducting analysis.

Table 1: Mean of sum of square errors obtained from E-SSM and SSM (benchmark)

Parameters	E-SSM	SSM
$\tilde{\Phi}$ (delta band)	3.33×10^{-5}	7.27×10^{-5}
$\tilde{\Phi}$ (alpha band)	1.41×10^{-5}	3.23×10^{-5}
$\tilde{\Phi}$ (gamma band)	1.69×10^{-5}	8.07×10^{-5}
τ^2	9.31×10^{-6}	2.03×10^{-4}
σ^2	1.93×10^{-1}	1.93×10^{-1}

6 Analysis of LFP data in an olfaction (nonspatial) sequence memory study

6.1 Data description

The LFPs dataset was obtained from an experiment searching for direct evidence of coding for the memory of sequential relationships among non-spatial events (Allen et al., 2016). During the course of experiment, rats were provided with series of five odors. All the odors were delivered in the same odor port. In each session, researchers presented the same sequence for multiple times. Each odor presentation was initiated by a nose poke and rats were required to correctly identify whether the odor was presented in the correct or incorrect sequence position (by holding their nose in the port until the signal or withdrawing before the signal, respectively). During the period of experiment, as rats performed the tasks, LFPs were recorded in the CA1 pyramidal layer of the dorsal hippocampus. In total, 22 tetrodes were implanted but LFPs were only analyzed from electrodes that exhibited task-critical single-cell activity (12 in this case). The LFPs dataset in this study comprise of 12 electrodes and

247 epochs. Each epoch is recorded over 1 second, aligned to port entry, sampled at 1000 Hertz and thus has $T = 1000$ time points.

6.2 Exploratory analysis

In our exploratory analysis, we are interested in two key goals: (1.) to determine how the original high-dimensional signals can be sufficiently represented by lower dimensional summary signals; and (2.) to assess if and how the spectral properties of the LFP signals evolve across epochs during the experiment.

To address the first question, we note the assertion in other studies (e.g., Makarova et al. (2014)) that the natural geometry of these neuronal assemblies gives rise to possible spatial segregation. This suggests that it is plausible to represent LFP data by lower dimensional summaries. In this nonspatial sequence memory study, we observe similar pattern across all the 12 electrodes. In Figure 10, although the power varies within each electrode, the synchrony of pattern across electrodes is still critical. For example, electrode 1 and 2 behave almost identically. Electrodes 10, 11 and 12 also follow the same pattern during the course of experiment. Moreover, as part of this exploratory analysis, we implemented spectral principal component analysis (Brillinger, 1964). This approach is widely used in the exploratory analysis of brain imaging data (Yuxiao Wang, 2016). Figure 11 presents the boxplots of the percentage of variability accounted by the first and third components. It can be shown that 3 components (mixture of delta, alpha and gamma bands) account for roughly 92% of the variability with the first component accounting for 70%. All these findings validate the assumption that the original LFPs can be projected into low dimensional source signals without substantial loss of information. In this paper, we will build on this preliminary analyses by giving a more specific characterization of these signal summaries or components using the AR(2) process.

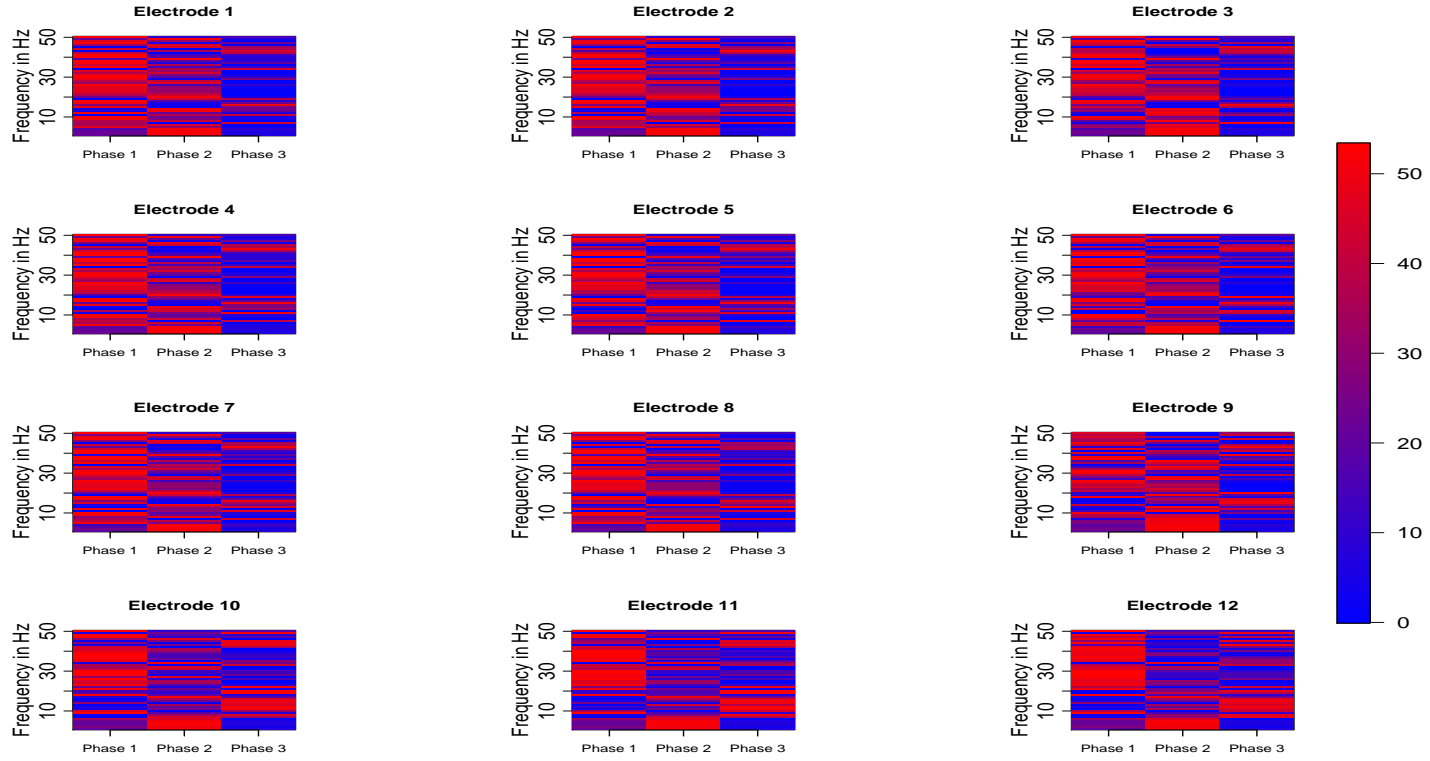


Figure 10: The evolution of the power spectrum across the duration of experiment. Each plot displays the estimated log power spectrum during the 3 phases: Phase 1 (epoch 1 - 80), Phase 2 (epoch 81 - 160) and Phase 3 (epoch 161 - 247). Frequency bands around particular hertz are present, which can be modeled as $AR(2)$.

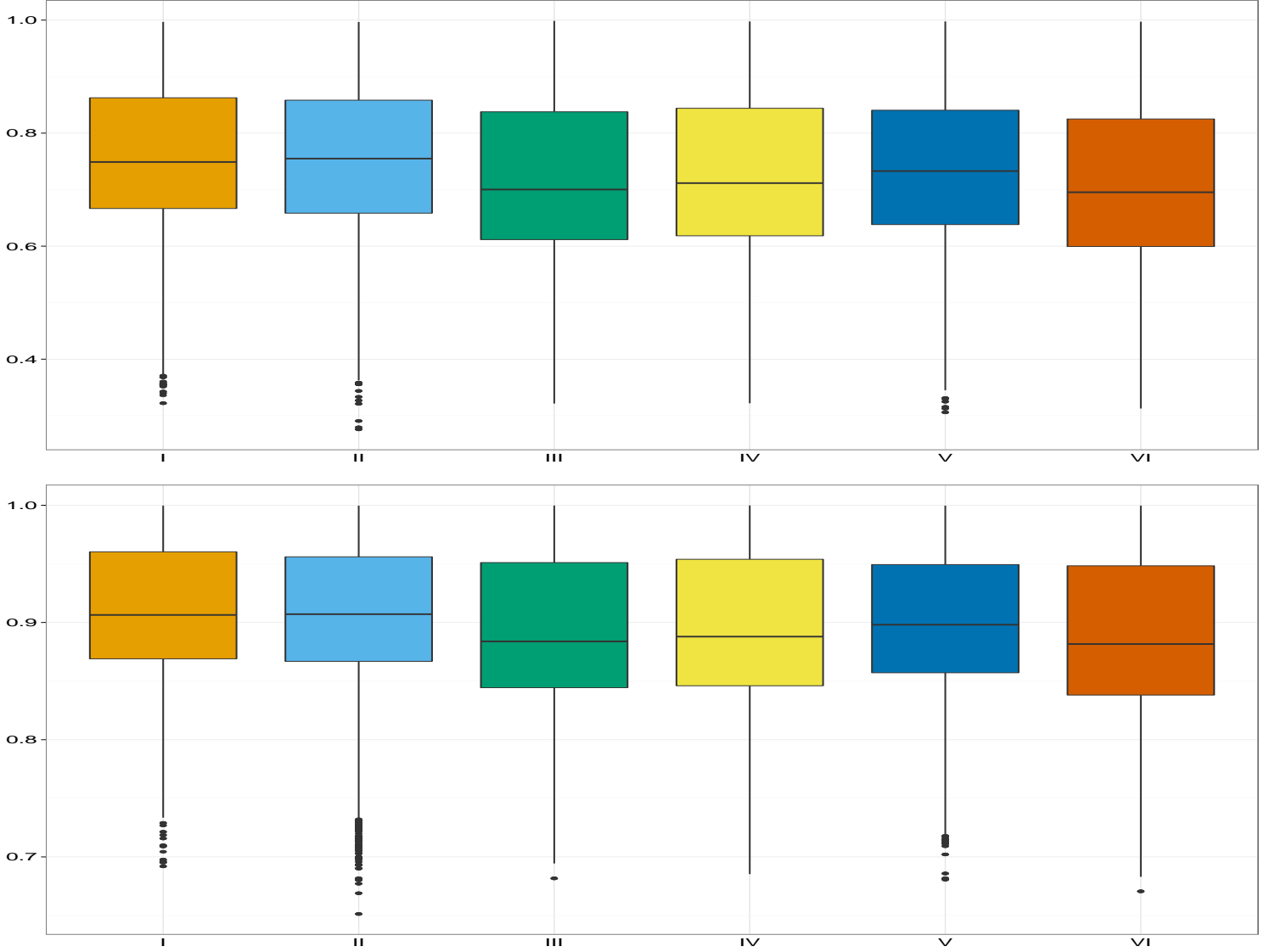


Figure 11: The boxplots of variance accounted by different components across different stages during the experiment. The results were obtained by conducting principal component analysis on frequency domain (Brillinger, 1964). Epochs in the entire experiment have been classified as 6 stages with each consisting of 40 epochs (Stage I: 1-40, II: 41-80, III: 81-120, IV: 121-160, V: 161-200, VI: 201-247). The first component is shown on top and the third is at the bottom. We could observe that about 90% of variance can be explained by three components.

To gain insights into addressing the second question, we examined the LFP traceplots of the first 15 epochs at electrode 7 (Figure 2). It is clear that signals across various elec-

trodes are highly associated as time evolves. Similarly, from the log periodogram boxplots in Figure 3 across all the frequencies, we notice that the powers are quite spread out, especially at lower frequencies and the two peaks around delta and slow gamma bands. The heatmap in Figure 4 demonstrates the dynamics from early, middle, and late stages of the whole session. Figure 10 shows the evolving of the power across all the electrodes particularly on delta, alpha, and gamma bands. It shows that higher frequency bands dominates in early and late phases, while lower frequency bands capture more power. In Figure 12, an interesting pattern emerges: the burst of gamma activity on Phase 1 of the epochs is not replicated at other phases. One possible interpretation is that odor sequence (on which the animals have had extensive training) is re-encoded early in each session, which requires high frequency (gamma) activity, but later in the session, gamma activity is regulated and other lower frequencies (delta and alpha) become more prominent. Inspired by all these results, a further study is necessary to uncover the latent lower dimensional source signals that drive the observed LFPs.

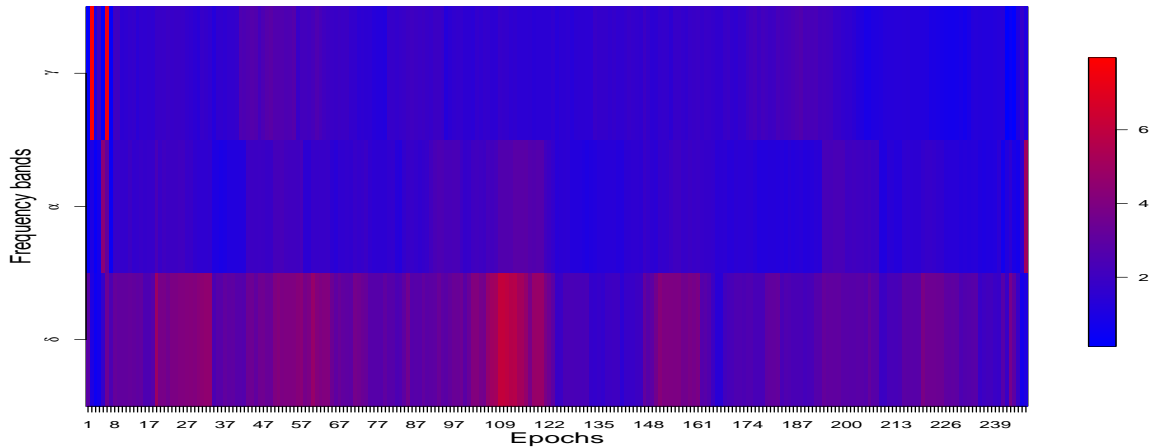


Figure 12: The evolution of power spectrum among delta (0-4 Hertz), alpha (8-12 Hertz) and gamma (30-35 Hertz) bands. Each band was averaged over all the electrodes.

6.3 Results and Discussion

We applied our proposed E-SSM method to this study. Figure 13 shows time series plots of modulus among all the three frequency bands as epochs evolve. In this plot, we could clearly identify the evolution of each individual module and a strong dependence in temporal space. Figure 14 displays the power of three latent source signals evolving during the period of experiment. We observe that the delta band captures the most power among all bands and is persistent across all phases. Gamma band power narrows down slightly towards the late phase. Alpha band attains its maximum power during the early phase and diminishes quickly in the middle stage and obtains more power in the end. There appear to be discontinuities in the delta, alpha and gamma power across the entire experiment. One interpretation to these results from the E-SSM analysis is that these on-off patterns could be just random variation. Another is that these are actual resetting of neuronal responses. This phenomenon of phase resetting in neurons is also observed in many biological oscillators. In fact, it is believed that phase resetting plays a role in promoting neural synchrony in various brain pathways. In either case, it is imperative to be cautious about blindly assuming that the neuronal process behaves identically across epochs. Doing so could produce misleading results.

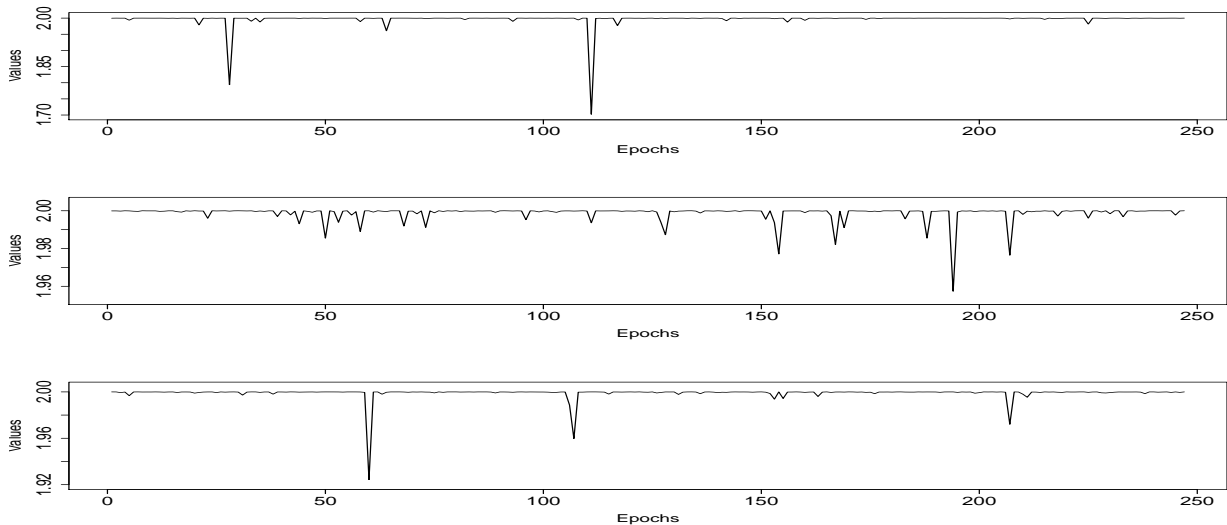


Figure 13: The time series plots of modulus corresponding to delta (above), alpha (middle) and gamma (bottom) frequency bands.

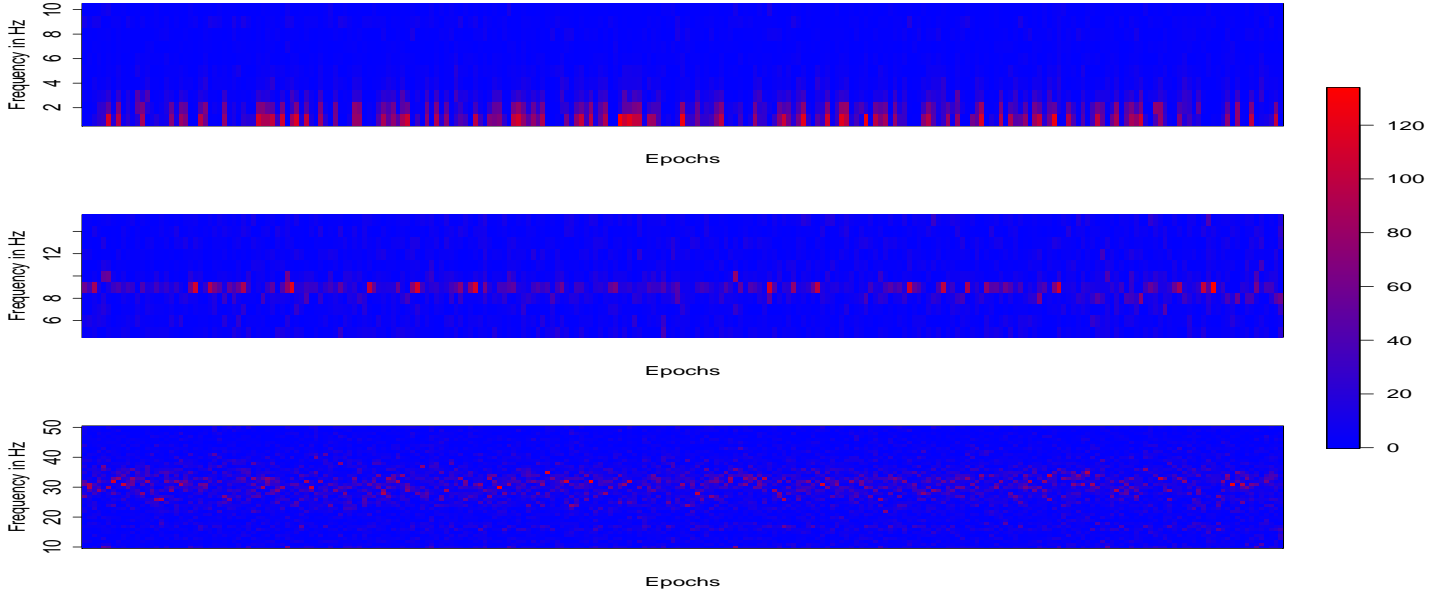


Figure 14: The periodograms of estimated latent $AR(2)$ processes corresponding to delta (top), alpha (middle) and gamma (bottom) frequency band.

We also study the “mixing” matrix to investigate how electrodes are associated across the three frequency bands. From Figure 15, at delta band, electrodes 1, 2, 4, 5, 7, 8 are likely to be linked in terms of large power. Electrodes 3, 9, 10, 11 and 12 share the lowest power. At alpha band, electrodes 4, 7 and 8 maintain the most power in contrast with electrodes 3, 9 - 12 that obtain the lowest power. This pattern of association may result from the anatomical connections. Similarly, at gamma band, electrodes are connected in the same way as alpha band. We also used a cluster analysis on the entries of “mixing” matrix to understand the connection among electrodes. Similar to the results shown in Figure 15, we are able to identify the same pattern in Figure 16, through the visualization of cluster analysis. At delta band, electrodes 1, 2, 4 - 8 share the same pattern while 9 - 12 are in the same cluster. Clusters at alpha and gamma bands are roughly identical, which coincide with the results in Figure 15. To the best of our knowledge, this approach (i.e., clustering of electrodes or nodes) has not been used previously for this kind of analysis. This has the potential for future explorations on synchrony among neuronal populations. Finally, we

note here that the specific parametric AR(2) structure in our E-SSM has facilitated ease of interpretation of the oscillatory activity of these sources.

We also examined model validation and diagnostics using the residuals. Sample auto-correlations (ACF) and partial auto-correlations (PACF) were computed from the residuals. Figure 17 shows an example of those values obtained from a representative electrode. We could easily observe the uncorrelated structure among the residuals. A p-value of 0.75 based on the Ljung-Box test also provides some evidence to suggest white noise residuals and thus conclude that the proposed E-SSM fits this LFP data well.

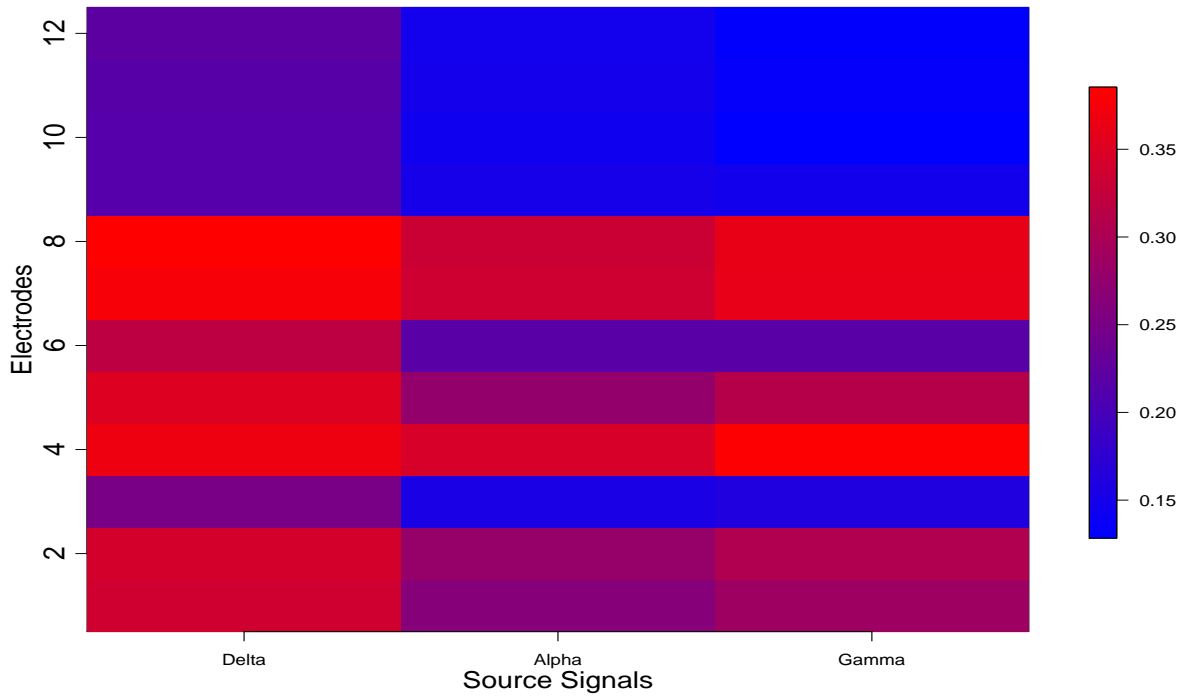


Figure 15: The estimated mixing matrix. Darker color represents heavier weights given by the latent processes (delta, alpha, gamma) on the LFPs.

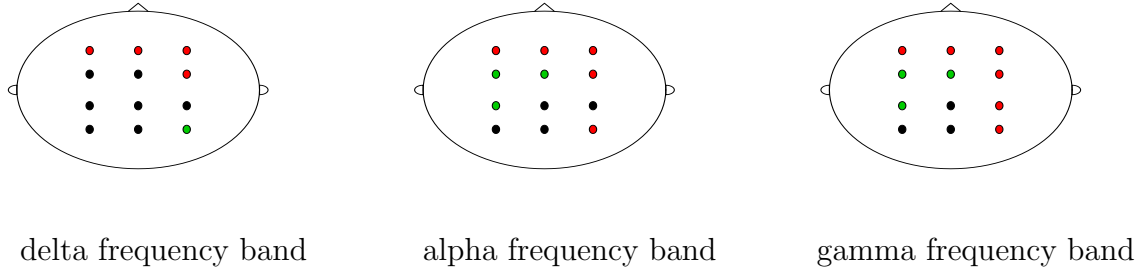


Figure 16: Cluster analysis results among all the three frequency bands.

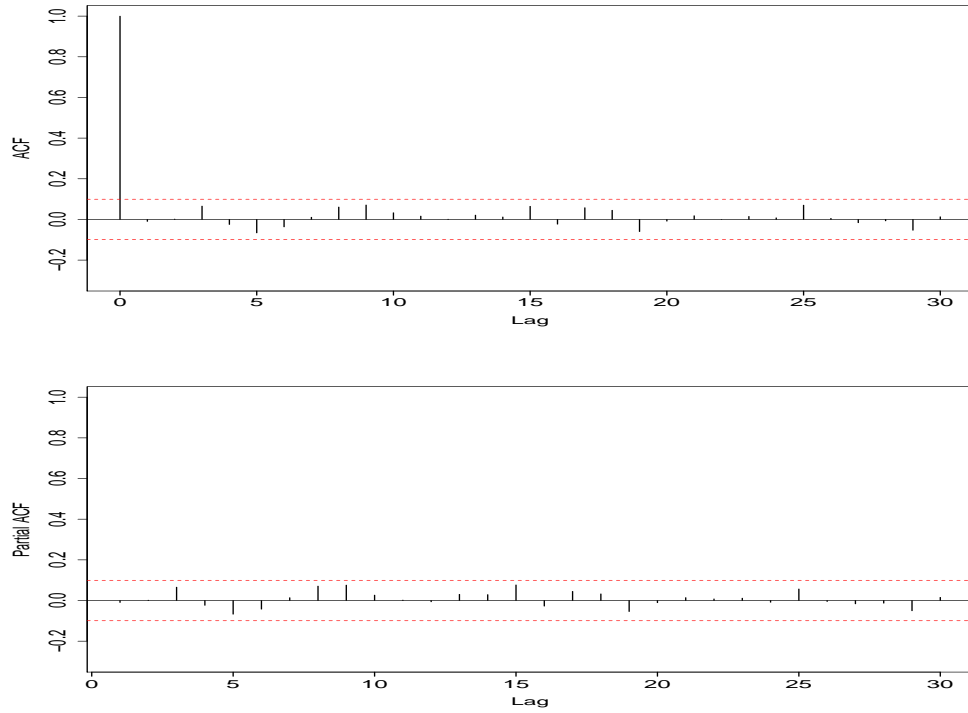


Figure 17: Top: Auto-correlation function (ACF) of the residual plots from electrode 1. Bottom: Partial auto-correlation function (PACF) of the residual plots from electrode 1. The dashed lines indicate the threshold for non-zero correlation. These plots, along with the Ljung-Box test for white noise ($p - value \approx 0.75$) suggest that the residuals are white noise and hence the E-SSM model fits the data well. These same plots were observed in all the other electrodes but we do not report them here due to space constraints.

7 Concluding remarks

In this paper, we have proposed an evolutionary state space model (E-SSM) that allows the latent source signals to evolve across epochs. The advantages of this methods are as follows: (1.) by introducing autoregressive structure in the latent source signals, it allows us to model the evolution of particular frequency bands in a parametric framework; (2.) the proposed method utilizes the autoregressive structure, which serves as a link between time and spectral domains, provides an approach of interpreting findings from both domains; (3.) compared to the existing methods, the proposed method is not computationally intensive since we have used ML and blocked resampling approaches for estimating the model parameters.

Although the results reported in this paper are quite promising, nevertheless, modeling the evolution/dynamics across epochs still remains a challenge in general. For example, in our current method, we ignored the subject specific random effects. Future extensions of our method should taken this into account. Moreover, future directions might involve incorporating different experimental conditions into our model to improve statistical inference.

References

- Allen, T. A., D. M. Salz, S. McKenzie, and N. J. Fortin (2016). Nonspatial sequence coding in cal neurons. *The Journal of Neuroscience* 36(5), 1547–1563.
- Arun, K. and S. Kung (1990). Balanced approximation of stochastic systems. *SIAM journal on matrix analysis and applications* 11(1), 42–68.
- Bell, A. J. and T. J. Sejnowski (1995). An information-maximization approach to blind separation and blind deconvolution. *Neural computation* 7(6), 1129–1159.
- Brillinger, D. (1964). A frequency approach to the techniques of principal components, factor analysis and canonical variates in the case of stationary time series. In *Invited Paper, Royal Statistical Society Conference, Cardiff Wales*. (Available at <http://stat-www.berkeley.edu/users/brill/papers.html>).

- Calhoun, V. D., J. Liu, and T. Adalı (2009). A review of group ica for fmri data and ica for joint inference of imaging, genetic, and erp data. *Neuroimage* 45(1), S163–S172.
- Einevoll, G. T., K. H. Pettersen, A. Devor, I. Ulbert, E. Halgren, and A. M. Dale (2007). Laminar population analysis: estimating firing rates and evoked synaptic activity from multielectrode recordings in rat barrel cortex. *Journal of neurophysiology* 97(3), 2174–2190.
- Fiecas, M. and H. Ombao (2016). Modeling the evolution of dynamic brain processes during an associative learning experiment. *Journal of the American Statistical Association* (just-accepted).
- Guo, Y. (2011). A general probabilistic model for group independent component analysis and its estimation methods. *Biometrics* 67(4), 1532–1542.
- Hamilton, J. D. (1994). *Time series analysis*, Volume 2. Princeton university press Princeton.
- Hyvärinen, A., J. Karhunen, and E. Oja (2004). *Independent component analysis*, Volume 46. John Wiley & Sons.
- Jiru, A. R. (2008). *Relationships between spectral peak frequencies of a causal AR (P) process and arguments of roots of the associated ar polynomial*. Ph. D. thesis, San Jose State University.
- Makarova, J., J. M. Ibarz, V. A. Makarov, N. Benito, and O. Herreras (2011). Parallel readout of pathway-specific inputs to laminated brain structures. *Frontiers in systems neuroscience* 5, 77.
- Makarova, J., T. Ortuño, A. Korovaichuk, J. Cudeiro, V. A. Makarov, C. Rivadulla, and O. Herreras (2014). Can pathway-specific lfps be obtained in cytoarchitectonically complex structures? *Frontiers in systems neuroscience* 8, 66.

- Michel, C., D. Lehmann, B. Henggeler, and D. Brandeis (1992). Localization of the sources of eeg delta, theta, alpha and beta frequency bands using the fft dipole approximation. *Electroencephalography and clinical neurophysiology* 82(1), 38–44.
- Mitzdorf, U. et al. (1985). *Current source-density method and application in cat cerebral cortex: investigation of evoked potentials and EEG phenomena*. American Physiological Society.
- Shumway, R. H. and D. S. Stoffer (2013). *Time series analysis and its applications*. Springer Science & Business Media.
- Whitmore, N. W. and S.-C. Lin (2016). Unmasking local activity within local field potentials (lfps) by removing distal electrical signals using independent component analysis. *NeuroImage* 132, 79–92.
- Yuxiao Wang, Chee-Ming Ting, H. O. (2016). Exploratory analysis of high dimensional time series with applications to multichannel electroencephalograms.
- Zhang, K. and A. Hyvärinen (2011). A general linear non-gaussian state-space model: Identifiability, identification, and applications. In *JMLR Workshop and Conference Proc., Asian Conf. on Machine Learning*, pp. 113–128.